J. Sustain. Metall. (2017) 3:543–550
DOI 10.1007/s40831-017-0130-8

RESEARCH ARTICLE

Effect of Crystallization on Microstructure and Elution Properties in Copper Slag

Hiromichi Takebe[1] · Sayuri Tomita[1] · Akira Saitoh[1] · Masayasu Kawahara[2] · Yuri Sueoka[1] · Masayuki Sakakibara[1]

Published online: 15 May 2017

Abstract Effects of cooling conditions on phase and microstructure in copper slag were studied. X-ray analysis of water-quenched slag shows noncrystalline, FeO-rich silicate phase, spherical copper loss particles, and a trace of crystalline phase. The slowly cooled slag in a furnace showed mainly fayalite and magnetite phases and SiO_2-rich (>65 mol%) alumino-silicate matrix phase with copper loss particles. The crystallized slag indicated less than one-tenth amount of the elution amounts of Pb and As in 1 mol/L HCl aqueous solution at room temperature, compared with the water-quenched slag. The formation of fayalite and magnetite phases resulted in the change of residual noncrystalline matrix from FeO-rich silicate to SiO_2-rich alumino-silicate compositions. Good stability against Pb and As dissolution in the HCl aqueous solution and SEM–EDS analysis for the crystallized copper slag suggested that Pb and As elements were present in the SiO_2-rich alumino-silicate matrix and embedded spherical particles of copper losses.

Keywords Slag · Crystallization · Microstructure · Chemical durability · Lead · Arsenic

The contributing editor for this article was I. Sohn.

✉ Hiromichi Takebe
takebe.hiromichi.mk@ehime-u.ac.jp

[1] Graduate School of Science and Engineering, Ehime University, 3 Bunkyo-cho, Matsuyama, Ehime 790-8577, Japan

[2] Graduate School of Science and Technology, Kumamoto University, Kurokami, Kumamoto 860-8555, Japan

Introduction

Copper smelting consists mainly of oxidation reaction of copper ore with SiO_2 and O_2. This process produces two types of melts: copper-concentrated sulfide matte and impurity-concentrated oxide slag at high temperatures, e.g., 1250–1300 °C [1]. Recently, it was found that lower concentration of Cu in copper ore results in the larger amounts of copper slag production per ton of copper produced during smelting process [2]. For sustainable copper process metallurgy, the utilization of copper slag has been one of important topics.

There are various potential applications of copper slag due to its stability and higher density, compared with natural sand, e.g., blend for concrete and asphalt, sand for artificial beach, roadbed, and ground, and as an iron-adjustment material in cement clinker [3, 4].

There is a guideline of JIS numbered K0058-1 and K0058-2. These are test methods for chemicals in slags: part 1 and part 2. Part2 (K0058-2) is the test method for acid-extractable contents of chemcials. Part2 is important for our study. The guideline shows that slag materials should satisfy the lower limit for the elution amounts of Pb and As fixed as ≤150 mg/kg in HCl aqueous solution after the standard sample preparation process and further elution tests [5]. However, it is known that water-quenched copper slag granule has higher Pb and As elution amounts of more than 150 mg/kg in the HCl aqueous solution [6].

In our recent research [6] and that of Kawahara and Komori [7], it was revealed separately that both the crystallized slag and the synthesized slag modified with higher SiO_2 concentrations have better stability against Pb and As dissolution in the HCl aqueous solution with a satisfaction of JIS K 0058-2.

The purpose of this study is to understand the variations of phase and microstructure under cooling conditions in copper slag. The elution properties of Pb and As in the water-quenched (X-ray noncrystalline) and crystallized copper slags are also compared. Finally, we study the relationships of the elution properties and microstructures between the quenched and crystallized copper slags.

Experimental Procedure

Sample Preparation

Copper slag granules were obtained, from some smelting companies, with ratios of 1.02–1.15 for total Fe(TFe)/SiO_2 in mass basis. One of the copper slag specimens was used for this study. Note that similar results to the ones we describe here were obtained for the other specimens of copper slags. Table 1 shows cation and sulfur contents of an as-received (water-quenched) copper slag. The content of oxygen was not included. Figure 1 shows the flow sheet of sample preparation process. The slag granule was sealed in a silica ampoule under the vacuum pressure of $\leq 5 \times 10^{-3}$ Pa. The sample was melted at 1250 °C for 1 h, and then cooled in a furnace at a rate of ~3 °C/min to room temperature. The ratios of Fe^{2+}/TFe were analyzed and found as 0.88 and 0.85 for the as-received and the slowly cooled slags by means of the chelatometric titration method, respectively.

Evaluation

Figure 2 shows the experimental flow chart to evaluate the elution properties of Pb and As in HCl aqueous solution. The flow chart used here is according to a previous study [7] and a guideline of JIS K 0058-2 [5]. The sample was crushed to sizes of 0.5–2.0 mm and weighed 6.0 g. The sample was immersed in 200 mL of 1 mol/L HCl aqueous solution contained in a plastic bottle. The solution with slag was shaken with a swing width of 45 mm and at a rotating speed of 200 rpm for 2 h. After shaking, the sample solution was allowed to settle for 30 min and centrifuged at a rate of 3000 rpm for 20 min. The upper clear solution was then filtrated by a membrane filter with a pore diameter of 0.45 μm. The filtrated liquid was adequately diluted to obtain desirable concentrations by adding 3% HNO_3 aqueous solution. The amounts of Pb and As in the elution liquid were evaluated at least three times for each sample by ICP-MS (VARIAN 820-MS), and the obtained values were averaged.

Noncrystalline/crystalline phases were detected by X-ray diffraction analysis (PANalytical, X'pert powder diffractometer), operating at 45 kV and 40 mA using Cu Kα radiation between 10 and 90 2θ. Before and after the elution tests, the microstructures of the slag samples were evaluated by SEM (JEOL, JSM-6510LV) with EDS analyzer (OXFORD, X-MAX50).

Table 1 Cation and sulfur contents of an as-received slag in this study

Element	TFe	Si	Al	Ca	Zn	S	Other elements[b]
(Mass%)[a]	38	17	1.8	1.4	1.6	0.45	<3.98

[a] Content of oxygen is not included

[b] Total content of metal elements: Mg, Pb, As, Bi, Cu, Mo, Na, K, P, Ti, Mn, Cd, Sn, Cr is shown. The content of each metal element was less than 1 mass%

Results

Phase and Microstructure

Figure 3 shows the XRD patterns of two types of slag samples: (1) water-quenched (as-received) and (2) re-melted in the vacuumed silica ampoule and cooled in a furnace at a rate of ~3 °C/min. The water-quenched sample shows X-ray halo pattern with a small trace of crystalline phase. The sample that was cooled relatively slowly in the furnace shows two crystalline phases of fayalite and magnetite. Similar phases have been observed in previous studies of copper smelting slags [8–10].

Figure 4 shows a typical SEM image of the water-quenched slag. The sample has a homogeneous matrix with a region of weak trace of heterogeneity and fine (<1 μm) and relatively large (>10 μm) spherical particles of copper loss. The gray elliptic particles near the copper losses contained Fe–Cr–Al–O elements and happened to be observed in this area. SEM–EDS analysis showed a typical example of matrix with a composition of $1.5K_2O$–

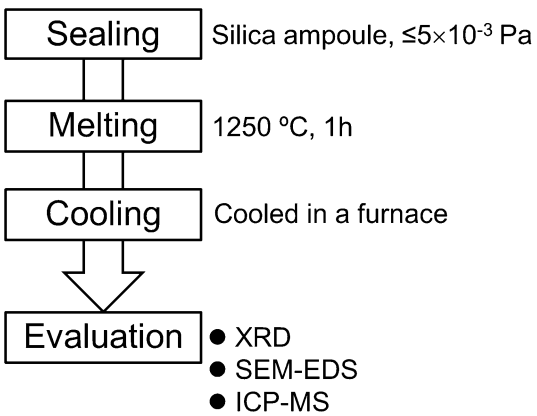

Fig. 1 Sample preparation process

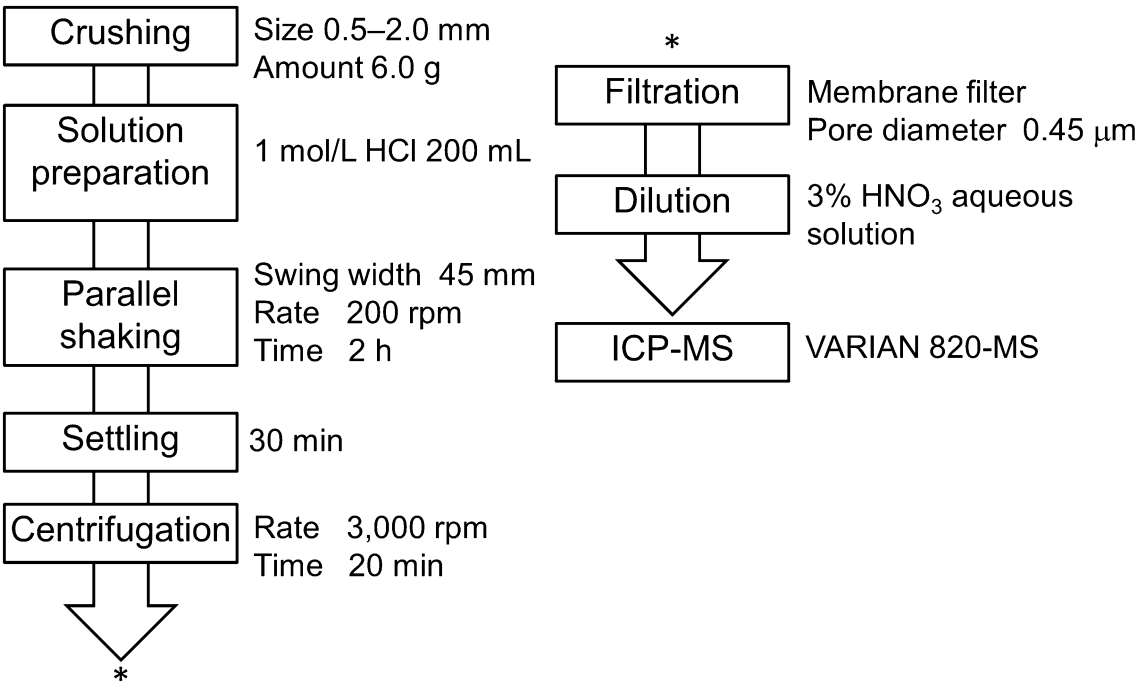

Fig. 2 Experimental flow to evaluate the acid-extractable contents of lead and arsenic in HCl aqueous solution under the guideline of JIS K0058-2:2005

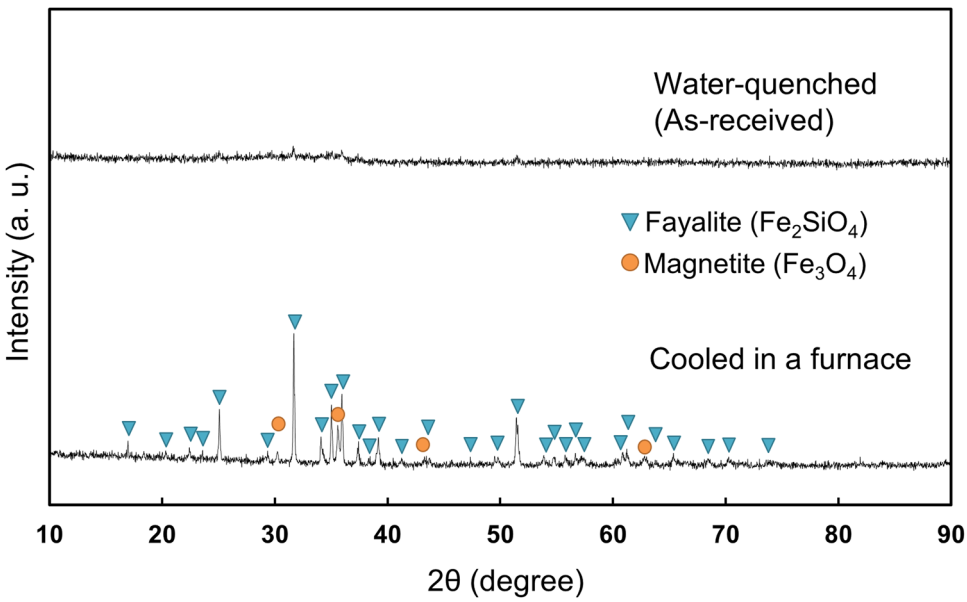

Fig. 3 XRD patterns of slag quenched into water and slag cooled in a furnace at a rate of 3 °C/min

53.1FeO–3.7Al_2O_3–41.7SiO_2 in molar ratio for major components (Table 2). The composition was an average of values obtained from eight locations in the matrix. It was also postulated that all the Fe ions exist in ferrous state in the water-quenched slag.

Figure 5 shows a typical SEM image of the slag cooled in the furnace. The SEM image shows clearly magnetite crystals and large fayalite aggregates (dark-gray area in Fig. 5). The alumino-silicate noncrystalline matrix (black area) is also found between fayalite aggregates. The SEM–EDS analysis indicated that the alumino-silicate matrix has a Al_2O_3- and SiO_2-rich composition of 2.9K_2O–1.4Na_2O–5.9CaO–13.5FeO–10.0Al_2O_3–66.3SiO_2 in molar ratio with a postulation of Fe ions existing in ferrous state (Table 2). The composition was estimated as an average of values for an example specimen from six locations in the

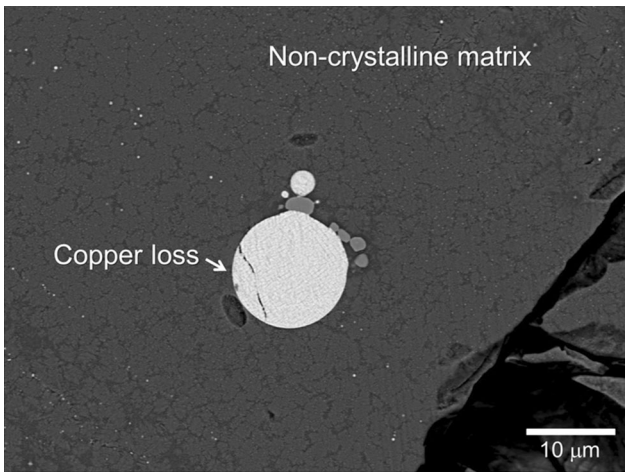

Fig. 4 A typical SEM image of the water-quenched copper slag

Table 2 Major components of noncrystalline matrix (NCM) phases remaining in the water-quenched (as-received) and furnace-cooled copper slags

Component (molar ratio)	Water-quenched	Cooled in the furnace
K_2O	1.5	2.9
Na_2O	–	1.4
CaO	–	5.9
FeO	53.1	13.5
Al_2O_3	3.7	10.0
SiO_2	41.7	66.3

It is postulated that all the Fe ions exist in ferrous state

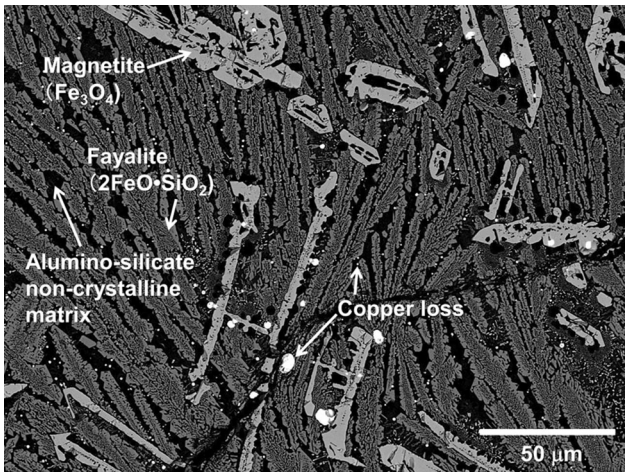

Fig. 5 A typical SEM image of the slag cooled in the furnace

noncrystalline matrix after the precipitation of magnetite and fayalite. The fine copper loss particles (<1 μm) were embedded in the alumino-silicate matrix. Moreover, in the slowly cooled copper slag, the SEM–EDS observation revealed that copper loss particles with >5 μm in diameter were sometimes composed of smaller Pb- and S-rich sulfide and As, Ni, Bi, and Sb-rich metallic areas in addition to Cu–Fe–S sulfide matte area. The copper loss particles may form thermodynamically stable crystalline phases after the slower cooling process. The alumino-silicate matrix also contains ~0.4% Pb and ~1%As, depending on the analyzed positions. Further study is necessary to evaluate microstructural distributions of toxic heavy metal elements: Pb and As.

Lead and Arsenic Elution Properties

Table 3 shows elution test results of two types of copper slag samples. All samples were dissolved completely into nitric acid to confirm the total contents of lead and arsenic. The left-hand side of Table 3 shows the contents of Pb and As constituents remaining within the same order due to compositional fluctuation during sample-selection and/or re-melting processes. It can be inferred from the extracted amounts of Pb and As in 1 mol/L HCl aqueous solution that the crystallized slag sample has less than one-tenth amount of the elution amounts of Pb and As elements compared to those of the water-quenched slag sample.

Figure 6 shows the XRD patterns of the water-quenched and crystallized slag samples after the elution test. The water-quenched sample shows a weak X-ray halo pattern with diffraction peaks of fayalite and magnetite. The XRD patterns of water-quenched slag before and after the elution test (Figs. 3, 6) may be related to the dissolution of noncrystalline matrix and the relative increase in the fraction of the crystalline phases. The sample cooled in the furnace shows the X-ray halo pattern with diffraction peaks of magnetite but without those of fayalite. The comparison of the XRD results before and after the elution test for the crystallized slag (Figs. 3, 6) suggests that the fayalite aggregates formed in the crystallized slag were selectively dissolved into the HCl aqueous solution during the elution test.

Figure 7 shows a typical SEM image of the water-quenched samples after the elution test. The pale areas pertain to the unreacted ones. On the contrary, dark areas

Table 3 The extracted contents of lead and arsenic in nitric acid for complete dissolution and in 1 mol/L HCl aqueous solution as per the guideline of JIS K 00258-2:2005

Dissolved completely	mg/kg	1 mol/L HCl	mg/kg
Pb		Pb	
Water-quenched	739	Water-quenched	368
Cooled in a furnace	861	Cooled in a furnace	28
As		As	
Water-quenched	345	Water-quenched	179
Cooled in a furnace	495	Cooled in a furnace	2

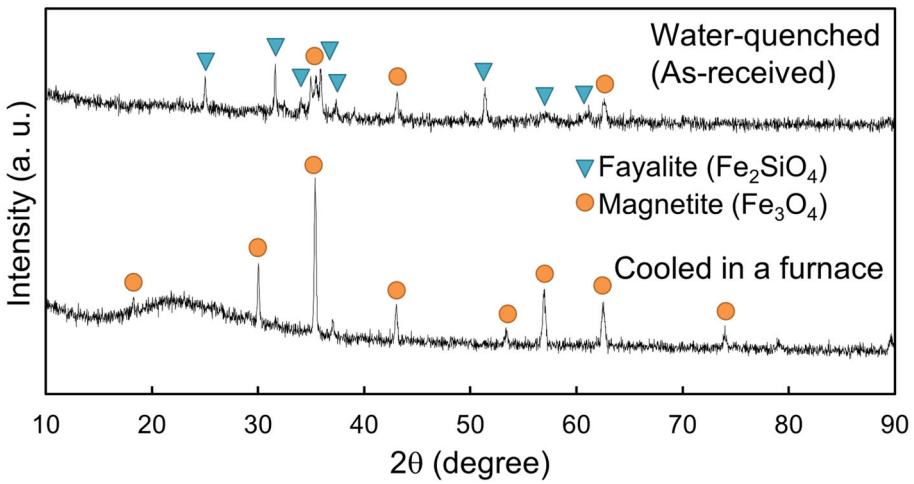

Fig. 6 XRD patterns of the copper slag samples: water-quenched and cooled in a furnace after the elution test

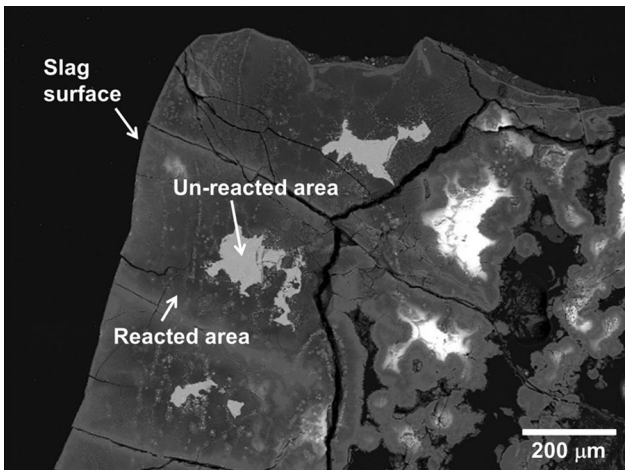

Fig. 7 A typical SEM image of the water-quenched copper slag sample after the elution test

extending from the surface are the regions pertaining to those that reacted with hydrochloric acid solution. The SEM–EDS analysis revealed that the difference in the compositions corresponded mainly to the concentration of iron. Iron in ferrous state (Fe^{2+}) in the noncrystalline matrix was probably dissolved into the hydrochloric acid.

Figure 8 shows the SEM–EDS images of the furnace-cooled slag. The result reveals that the selective dissolution of iron occurs only at the area of fayalite aggregates. The SEM image indicates the area of fayalite aggregates, and the morphology shows the trace of selective dissolution of iron present in ferrous state. Magnetite crystals with both ferrous and ferric states and alumino-silicate noncrystalline area with several copper loss particles still remain after the elution test. This microstructural observation well corresponds to the XRD pattern consisting of X-ray halo patterns and the diffraction peaks of magnetite for the furnace-cooled slag, as shown in Fig. 6.

Discussion

Figure 9 shows the schematic diagrams of microstructures of water-quenched and crystallized copper slags. The water-quenched slag shows X-ray halo pattern mainly (Fig. 3). The composition of the noncrystalline matrix was that of FeO-rich silicate with small amounts of potassium and aluminum oxides (Table 2). This matrix included lead and arsenic. These heavy metal elements were also detected on some spherical particles of copper loss.

When the copper slag was cooled at the slower cooling rate, the slag was crystallized with the formation of fayalite and magnetite phases, and this resulted in the change of residual matrix from FeO-rich silicate to silica-rich alumino-silicate compositions. This is similar to the composition of alumino-silicate glasses with good durability and mechanical properties, which have been used for smartphone and tablet screens [11]. The lead and arsenic elements were probably distributed in this alumino-silicate noncrystalline matrix and in some of spherical particles of copper loss embedded in the matrix.

The lead (Pb) is classified as a modifier for its contribution toward glass formation in a similar manner to that of alkali ions [12]. Moreover, $PbO–SiO_2$ binary system has a wide range of glass formation up to 95 mol% PbO [13]. The lead oxide is easily incorporated into the silicate network with modification occurring homogeneously and continuously due to the formation of covalent Pb–O–Si bonds. It is known that As_2O_3 shows a behavior similar to that of Sb_2O_3 used as a fining agent for gaseous bubble removal in multicomponent silicate glasses [14]. The NMR results indicated that antimony oxide with a molecular mixture of trigonal planar and tetrahedrally coordinated units showed the increase of silicate network connectivity to form covalent Sb–O–Si bonds [15]. The arsenic oxide may also contribute to the enhancement of silicate network

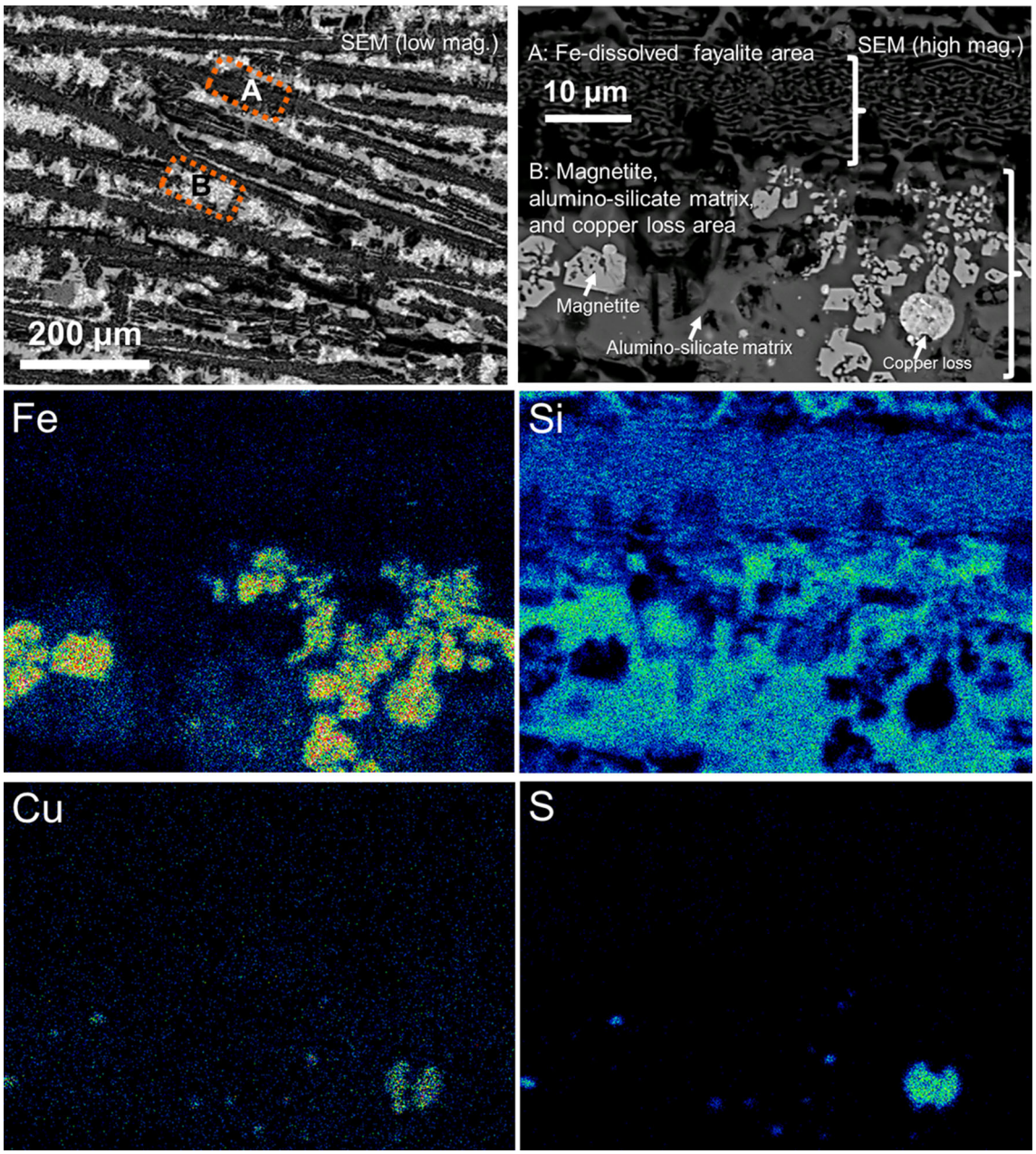

Fig. 8 SEM–EDS images of the copper slag cooled in the furnace after the elution test

as a mixture of AsO_3 and $[AsO_4]^-$ units charge-compensated by modifier cations with the formation of As–O–Si bonds.

The microstructure of the crystallized slag after the elution test revealed that FeO (ferrous oxide) in fayalite (Fe_2SiO_4) phase and coarse Cu–Fe–S spherical particles existing near the fayalite pillars with >10 μm in diameter were selectively dissolved into 1 N HCl aqueous solution. The result is summarized as per the following equation:

Fe_2SiO_4 + NCM (noncrystalline matrix of alumino-silicate) + Fe_3O_4 + Cu–Fe–S (copper losses) → FeO↓ (in Fe_2SiO_4, dissolved), Cu–Fe–S↓ (copper losses attached the fayalite aggregates, dissolved) + NCM (alumino-silicate) + Fe_3O_4 + Cu–Fe–S (copper loss particles embedded in the NCM and magnetite precipitates).

In other words, the suppression of Pb and As elutions in the crystallized slag confirms that the formation of Fe_2SiO_4 and Fe_3O_4 phases results in the compositional change of the NCM with regard to Al_2O_3 and SiO_2-rich alumino-silicates including Pb and As elements. For instance, the SEM–EDS analysis showed that the chemical composition of NCM with molar ratio in water-quenched slag was

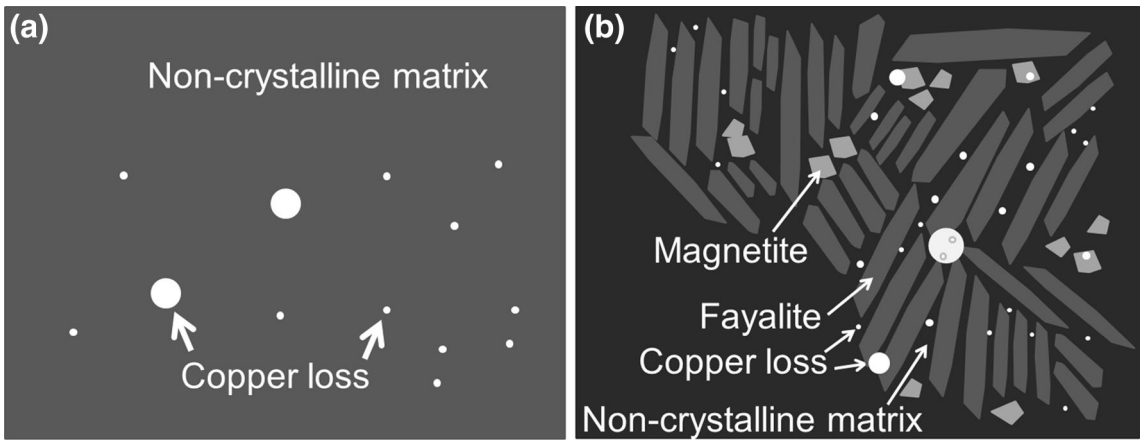

Fig. 9 Schematic diagrams of microstructures of copper slags: **a** water-quenched and **b** cooled in the furnace

$1.5K_2O$–53.1FeO–$3.7Al_2O_3$–$41.1SiO_2$ and that of NCM in the crystallized slag was $1.4Na_2O$–$2.9K_2O$–5.9CaO–13.5FeO–$10.0Al_2O_3$–$66.3SiO_2$ (Table 2). This result also supports a previous report that the increase of SiO_2 content in a modified-copper slag reduced the Pb and As elution amounts in 1 N HCl aqueous solution [7]. The corrosion of silicate glasses in acidic solution predominantly occurred at nonbridging oxygen sites by means of the proton (H^+) substitution for modifier cations [16]. The higher ($\geq$60 mol%) concentration of SiO_2 in alumino-silicate and silica glasses contributes toward the good chemical durability against acidic solution, resulting from the three-dimensional silicate network with lower concentrations of nonbridging oxygen sites [17].

The controlled cooling rate employed to crystallize the copper slag is supposed to be one of effective ways to modify the elution properties of Pb and As in HCl aqueous solution. Dry slag atomization [18, 19] and other processes with slower and controlled cooling rates are considered for the crystallization of copper slag with macroscopic morphology control for various future applications.

Conclusions

Copper slag in smelting process was re-melted in the vacuum-sealed ampoule and cooled with a slow rate for crystallization. Slower cooling to form the fayalite and magnetite phases results in the formation of SiO_2-rich alumino-silicate noncrystalline matrix.

The crystallized copper slag with SiO_2-rich (>65 mol%) noncrystalline matrix probably containing lead and arsenic elements has less than one-tenth amount of the elution amounts of Pb and As in 1 mol/L HCl aqueous solution, compared with the water-quenched copper slag as specified in the guideline of JIS K 0058-2 as a test method for acid-extractable contents of chemicals.

Acknowledgements This research was partly supported by the Grants-in-Aid for Scientific Research (B) No. 15H041617 from the Ministry of Education, Science and Culture of the Japanese Government. The authors also thank the foundation of the Japan Mining Industry Association, 2013–2015.

References

1. Gorai B, Jana RK (2003) Characteristics and utilization of copper slag—a review. Resour Conserv Recycl 39:299–313. doi:10.1016/S0921-3449(02)00171-4
2. Northey S, Haque N, Mudd G (2013) Using sustainability reporting to assess the environmental footprint of copper mining. J Clean Prod 40:118–128. doi:10.1016/j.jclepro.2012.09.027
3. Shi C, Meyer C, Behnood A (2008) Utilization of copper slag in cement and concrete. Resour Conserv Recycl 52:1115–1120. doi:10.1016/j.resconrec.2008.06.008
4. Tamil Selvi P, Lakshmi Narayani P, Ramya G (2014) Experimental study on concrete using copper slag as replacement materials of fine aggregate. J Civil Environ Eng 4:1000156. doi:10.4172/2165-784X.10000156
5. http://www.jisc.go.jp/newstopics/2012/201203slag_hokokusho.pdf
6. Takebe H, Tomita S, Okada A (2016) Effect of cooling rate on phase and microstructure in copper slag. Proc Copper 2016 RW2-4
7. Kawahara M, Komori S (2013) Elution property of heavy metals from copper slag. J MMIJ 129:192–196
8. Fan Y, Shibata E, Iizuka A, Nakamura T (2014) Crystallization behaviors of copper slag studied using time-temperature-transformation diagram. Mater Trans 55:958–963. doi:10.2320/matertrans.M-M2014819
9. Fernández-Caliani JC, Ríos G, Martínez J, Jiménez F (2012) Occurrence and speciation of copper in slags obtained during the pyrometallurgical processing of chalcopyrite concentrates at the Huelva smelter (Spain). J Min Metall Sect B 48:161–171. doi:10.2298/JMMB111111027F
10. Guo Z, Zhu D, Pan J, Wu T, Zhang F (2016) Improving beneficiation of copper and iron from copper slag by modifying the molten copper slag. Metals 6(86):1–17. doi:10.3390/met6040086
11. Wang M, Wang B, Bechgaard TK, Mauro JC, Rzoska SJ, Bockowski M, Smedskjaer MM, Bauchy M (2016) Crucial effect of angular flexibility on the fracture toughness and nano-ductility of aluminosilicate glasses. J Non Cryst Solids 454:46–51. doi:10.1016/j.jnoncrysol.2016.10.020

12. Stanworth JE (1953) Physical properties of glass. Oxford University Press, London
13. Yanagase T, Suginohara Y (1970) Studies on contribution of vitreous silicate by infrared absorption spectra. Trans Jpn Inst Metals 11:400–403
14. Keber E, Frishcat G (1992) Influence of batch moisture and atmosphere on the melting behavior of As_2O_3- and Sb_2O_3-containing glasses. Glastech Ber 65:64–66
15. Wood JG, Prabakar S, Mueller KT, Pantano CG (2004) The effects of antimony oxide on the structure of alkaline-earth alumino borosilicate glasses. J Non Cryst Solids 349:276–284. doi:10.1016/j.jnoncrysol.2004.08.186
16. Hamilton JP, Pantano CG (1997) Effects of glass structure on the corrosion behavior of sodium-aluminosilicate glasses. J Non Cryst Solids 222:167–174
17. Takahashi S, Neuville DR, Takebe H (2015) Thermal properties, density and structure of percalcic and peraluminus $CaO–Al_2O_3–SiO_2$ glasses. J Non Cryst Solids 411:5–12. doi:10.1016/j.jnoncrysol.2014.12.019
18. Zuber M, Heuer A, Zervos J, Garía JO, González L, Oria IR, Ransanz GR, Oh S-Y, Lai L, So C, Mostaghel S, Francey S, Faucher S (2016) Dry slag atomization of copper slags for iron silicate production. Proc Copper 2016 PY23-1
19. Maruoka N, Mizuochi T, Purwanto H, Akiyama T (2004) Feasibility study for recovering waste heat in the steelmaking industry using a chemical recuperator. ISIJ Int 44:257–262